Prediction and analysis of high velocity oxy fuel (HVOF) sprayed coating using artificial neural network

Meimei Liu, Zexin Yu, Yicha Zhang, Hongjian Wu, Hanlin Liao, Sihao Deng

Prediction and analysis of high velocity oxy fuel (HVOF) sprayed coating using artificial neural network

Meimei LIU[a1], Zexin YU[a1], Yicha ZHANG[b], Hongjian WU[a], Hanlin LIAO[a], Sihao DENG*[a]

a: *ICB-LERMPS UMR 6303, CNRS, UTBM, Université de Bourgogne Franche-Comté, 90010 Belfort, France*

b: *ICB-COMM UMR 6303, CNRS, UTBM, Université de Bourgogne Franche-Comté, 90010 Belfort, France*

* Corresponding author: sihao.deng@utbm.fr (Sihao DENG)

1: These authors contributed equally for this work

Abstract: Thermal spray comprises a group of coating processes for coating manufacturing in which metallic or nonmetallic materials are deposited in a molten or semi-molten condition. Most often, the coating properties are significantly influenced by the operating parameters. However, obtaining a comprehensive modeling or analytical analysis of the thermal spray process is too difficult to be practical due to the complex chemical and thermodynamic reactions. Accordingly, the present study aims at applying an artificial neural network (ANN) model to predict the HVOF sprayed Cr3C2−25NiCr coatings and analyze the influence of operating parameters regardless of the intermediate process. The process parameters, which were automatically recorded by the homemade HVOF spray system during the spray process, were served as the inputs for the ANN model. Then, the porosity, microhardness and wear rate of coatings were measured and considered as targets for the ANN model. After configuring and training procedure of the model, the predicted results were compared to the results of experimental data. The good consistency found between these results permits to verify the reliability and accuracy of the trained ANN model. Additionally, the mean impact value (MIV) analysis was conducted to quantitatively explore the relative significance of each input variable for improving the effective prediction.

Keywords: HVOF spray; ANN model; MIV analysis; Cr3C2−25NiCr coatings

1. Introduction

Thermal spray comprises a group of coating processes for coating manufacturing in which finely divided metallic or nonmetallic materials are deposited in a molten or semi-molten condition [1]. The high-velocity oxy-fuel process (HVOF) has been regarded as one of the most efficient techniques for depositing high-performance coatings at moderate cost [2]. In this process, the feedstock powders are sent into the combustion chamber by the carrier gas and heated at high temperature by the combustion of mixture gas. The heated or melted particles are accelerated by the combustible gases to achieve the supersonic velocity when they go through the de Laval nozzle, and then deposit on the substrate to form a coating [3,4]. Dense and homogenous coatings, having low porosity, high hardness and high wear resistance are therefore formed. The HVOF sprayed coatings, such as NiCr-based [5–7] or WC-Co-based [8,9] coatings, have been widely applied to improve surface quality and performance of metal parts for varied industrial applications, owing to their excellent chemical and mechanical performance, such as high oxidation resistance, corrosion resistance, and wear resistance.

The coating performances are highly dependent on the operating parameters of the HVOF process. Fuel flow rate, spraying distance and oxygen flow rate were examined as the most important HVOF process parameters affecting the characteristics of in-flight particles [10]. Higher particle velocity would contribute to increasing the hardness and cavitation erosion resistance of the coatings [11]. Mechanical properties of HVOF sprayed Cr3C2-25NiCr coatings showed a strong dependence on microstructural features which were closely linked to selected processing parameters [12]. Variations in oxygen flow rate and fuel flow rate have had an effect on the velocity and temperature of the particles in flight, which therefore changes the properties of the HVOF sprayed coatings [13]. the Taguchi design method, which is an initial solution to identify the optimized process parameters and distinguish the major and minor factors, is the most widely used method to estimate the influences of the HVOF process parameters on the

coating properties [14–16]. However, it may fail to achieve the precise optimal parameters since the coating quality is normally influenced by a combined effect of many HVOF process parameters. Numerical modeling and simulation have also been widely employed to simulate and control the spray process [17–19], which commonly pay more attention to investigating the development of the combustion and spray process. However, due to the complex multi-physical phenomenon of the thermal spray process, numerical modeling has difficulties to modeling the real behaviors. Therefore, a method for careful analysis, prediction, and optimization of the HVOF sprayed coatings is necessary.

The artificial neural networks (ANN) is a computational model inspired by the organization, interconnection and the way information is processed of the biological neural networks constituting animal brains [20]. An ANN is similarly composed of processing elements called artificial neurons (analogous to biological neurons) and connection coefficients called weights (analogous to synapses) [21,22]. It can self-regulate and fit various nonlinearities in the data series through training and learning, which provides a method with high quality and efficiency to calculate the optimal conditions for manufacturing processes [23]. This method is mainly used when the relationship among the studied variables is complex or when the knowledge of the physical correlations is limited. Thermal spraying technologies are such kinds of processes containing complex chemical and thermodynamic reactions, which need to be researched with a powerful computational model, such as the ANN model. However, it is hard or costly to capture enough data sets of the thermal spraying processes and coatings, especially to collect enough data of the coating properties. Therefore, the application of the shallow ANN model, which normally contains less than three hidden layers for relatively less data applications, has also attracted increased attentions in the thermal spraying technique. Examples of applications of ANN models in thermal spray were lists in Table.I [24–31]. Most of the works were concentrated on the atmospheric plasma spray (APS) process and the ANN method has been relatively less used in

HVOF sprays. There are limited researches about the investigation of the HVOF spray process by applying the ANN model. Additionally, the relative importance of each input variable in the ANN model has seldom been studied for the thermal spray process.

In this study, the HVOF spray experiments and corresponding tests have been carried out to create the data set for the training, validation and test of the ANN model. The ANN model has been introduced to thoroughly study the HVOF spray process and has been applied to correlate the process parameters of HVOF spray ((served as inputs for the ANN model)) to the mechanical performance of coatings(served as targets for the ANN model). The reliability and accuracy of the ANN model have been verified by further experiments. Moreover, mean impact value (MIV) based analysis has been conducted to quantitatively explore the relative importance of each input variable for the improvement of the mechanical performance of coatings

2. Experimental and characterization procedures

2.1 Spray materials and coating fabrication

The commercial available Cr3C2-25(Ni20Cr) (METCO 81 VF-NS: Oerlikon Metco AG, Wohlen, Switzerland) powder were used as feedstock in this study. The powder was received with a nominal particle size distribution of-45+5 μm.

The HVOF spray experiments were carried out with a homemade Diamond Jet spray system. It characterizes with a recompiled control system programmed by using the programmable logic controller (B&R Industrial Automation GmbH, Eggelsberg, Austria) and a commercial DJ-2701 hybrid gun (Sulzer-Metco, Westbury, NY). A six-axis industrial robot IRB2600-20 (ABB, Sweden) was employed to fix the gun. 316L stainless steel plates (Ø25mm×10mm) were used as the substrates, which were grit-blasted and then ultrasonically cleaned in ethanol for 10 min before experiment. Methane was used as the fuel gas in this work. Experiments have been carried out by varying three process parameters, namely O_2 flow rate, CH_4 flow rate and stand-off distance. The CH_4 flow rate varied from 120 to 200 slpm and O_2 flow

rate from 200 to 240 slpm. The stand-off distance was set as 280 and 320 mm. The HVOF spray process parameters are listed in Table.II.

2.2 Coating characterization

The microhardness of coatings was measured on the coating cross section by a Vickers microhardness indenter (Leiz-Wetzlar, Germany) with a load of 300 gf (e.t. 2.94 N) and a dwelling time of 25 s. twenty indentations were randomly measured and thereby give an average microhardness value for each coating.

In order to calculate the porosity of coatings, the cross-sectional microstructure of prepared coatings was examined by a scanning electron microscope (SEM, JSM-5800LV, JEOL) with a secondary electronic mode. More than ten consecutive pictures were captured and an average value was calculated by using the imaging software (Image J).

Dry sliding wear tests were carried out in a CSEM tribometer (Switzerland) having a ball-on-disc configuration. The tests were performed at atmospheric environment with temperature of 15-20℃ and humidity of 40-50%. Al_2O_3 ball (6 mm diameter) was employed as the counterpart material and was cleaned with alcohol before test. the test were conducted at the same sliding condition with a load of 5 N, a rotation radius of 7 mm, a linear rotation speed of 10 mm/s and a sliding distance of 500 m. The cross-sectional profiles of the worn track were measured using a profilometer (Altisurf 500, France). At least ten profiles were conducted to give an average wear volume. Then the wear rate of the samples, which stands for the amount of material removed from the surface and uses to evaluate the wear resistance of coatings, is expressed by:

$$K = \frac{\Delta V}{SF_N} \tag{1}$$

, where $\Delta V$is the volume loss of the material [mm^3], S is the sliding distance [m] and F_N is the applied normal load [N].

The samples for all the tests, i.e. the samples for measuring the microhardness and porosity, the surface of as-sprayed coatings for the dry sliding tribological test, were prepared with the same sequential procedure of grinding with P220 SiC paper and MD-Largo disc, and polishing with 3μm diamond suspension and 0.04μm non-drying colloidal silica suspension.

3. Simulation model

Thermal spray is considered as a non-linear problem taking its operating conditions and properties into account. An ANN model is a powerful statistical method to recognize the correlations between the parameters of a complex modeling or generalization problem and its response, such as pattern recognition and nonlinear system identification and control [32]. In this section, an ANN model has been configured and trained to predict the coating properties (microhardness, porosity and wear rate of coatings) from the process parameters (stand-off distance, oxygen flow rate, and fuel flow rate). The development of the ANN model is described as following.

3.1 Data collection and pre-processing

For configuration, training and validation of the ANN model, firstly, the operating parameters and test results were collected and pre-processed. A database of 120 data derived from 20 set of HVOF experiments and related tests was collected. Three process parameters, oxygen flow rate ($Q(O_2)$), fuel flow rate ($Q(CH_4)$), and stand-off distance(Dis), were served as the inputs for the ANN model. Meanwhile, the microhardness, porosity and wear rate of the coatings were used as the targets. The experimental values of the inputs and outputs were tabulated in Table.III. for the pre-processing, the data would be normalized according to Eq. (2) to fall in the range [-1, 1] in order to avoid the calculation error related to different parameter magnitudes [33]. All the data was randomly divided into three set according the data division function of “dividerand”. The ratio of the training set, testing set and validation set were 70%, 15% and 15% respectively.

$$X_{NORM} = \frac{X - X_{MIN}}{X_{MAX} - X_{MIN}} \quad (2)$$

, where, X_{NORM} is the normalized value; X is the experimental value; X_{MAX}, X_{MIN} are the maximum and the minimum of the experimental values in the data set.

3.2 Establishing, training, and validation of the ANN model

Once the data has been allocated, the next step is to configure the network and conduct the training of the network.

Since both of the input and target variables of network are three, the numbers of neuron in input and output layers were accordingly set as three neurons. However, there is no general rule to precise the number of neurons in the hidden layers. The number of hidden layers and the number of neuron in the hidden layer are determined considering the accuracy of the trained model and the complexity of network structure. Normally, higher accuracy with lesser number of hidden layers and neurons in the hidden layer is expected. Consequently, An ANN model with two hidden layers and ten neurons in both of these two hidden layers was chosen, the architecture of which was shown in Fig.1. The accuracy of the model can be measured by the correlation coefficient (R) value, which provides an understanding about how well the outputs of the trained model fit the actual experimental results. If R = 1, this indicates that there is an exact linear relationship between the outputs and targets. If R is close to zero, then there is no linear relationship between outputs and targets.

The training of the ANN model in this work was conducted in a supervised manner, using the back-propagation method. It is a typical learning technique comprised of a multilayer feed forward neural network trained by the error BP algorithms [34]. The inputs are sent forward via transfer function and the errors between the predicted outputs of using the network weights and the targets of the training set (experimental data) are calculated. The differences are propagated backward and the error network is feedback by adjusting the weights in order to minimize the

errors. The task of determining the set of values for the weights that minimizes an error function is so-called training. The values of the weights and biases of the network are tuned to optimize network performance during the process of training, as defined by the network performance function. In this study, the performance function for networks is mean square error (MSE) - the average squared error between the networks outputs and the experimental result. It is defined as follows [35]:

$$MSE = \frac{1}{N}\sum_{i=1}^{N}(e_i)^2 = \frac{1}{N}\sum_{i=1}^{N}(t_i - a_i)^2 \quad (3)$$

, where, t_i is the experimental result; a_i is the network predicted result; e_i is the difference between the experimental result and the network predicted result; N is the number of the data sets.

The ANN model was trained and tested in Matlab (MathWorks, Natick, MA, USA). The Log-sigmoid transfer function (logsig) was selected as the transfer function for hidden layers, the Linear transfer function (purelin) as the transfer function for output layer, and Levenberg-Marquadt Back-propagation (trainlm) as the training function. The functions used were summarized in Table.IV.

3.3 MIV analysis approach

Introducing an appropriate method to analyze the significance of each input variable taking into account the error of the input variables is meaningful. MIV based analysis provides such a method for ANN model to explore the relative importance of each input variable for the improvement of the prediction performance.

The MIV method, firstly proposed by Dombi GW in biomedical field, is used to choose parameters or analyze the independent variables that have a great impact on the dependent variables in an ANN [36]. Hereafter, it has been widely employed to quantitatively feature

analysis in the machine learning applications [37,38]. The process of MIV based analysis is as follows [39]:

(1) Obtaining the trained ANN model with the input (X) in the data set, as shown in Eq. (4).

$$X = \begin{bmatrix} x_{11} & x_{12} & \cdots & x_{1m} \\ x_{21} & x_{22} & \ldots & x_{2m} \\ \vdots & \vdots & \ddots & \vdots \\ x_{n1} & x_{n2} & \cdots & x_{nm} \end{bmatrix} \tag{4}$$

,where, n is the number of the input variables, m is the number of values of each variable.

(2) The ith variable in X is added and reduced by 10% to form two new inputs, $X_i(1)$ and $X_i(2)$, as displayed in Eq. (5) and Eq. (6).

$$X_i(1) = \begin{bmatrix} x_{11} & x_{12} & \ldots & x_{1m} \\ \vdots & \vdots & & \vdots \\ x_{i1}(1+10\%) & x_{i2}(1+10\%) & \cdots & x_{im}(1+10\%) \\ \vdots & \vdots & & \vdots \\ x_{n1} & x_{n2} & \ldots & x_{nm} \end{bmatrix} \tag{5}$$

$$X_i(2) = \begin{bmatrix} x_{11} & x_{12} & \ldots & x_{1m} \\ \vdots & \vdots & & \vdots \\ x_{i1}(1-10\%) & x_{i2}(1-10\%) & \cdots & x_{im}(1-10\%) \\ \vdots & \vdots & & \vdots \\ x_{n1} & x_{n2} & \ldots & x_{nm} \end{bmatrix} \tag{6}$$

(3) These two new inputs are used for simulation with the trained model. The simulated outputs, i.e. $Y_i(1)$ and $Y_i(2)$, based on $X_i(1)$ and $X_i(2)$ are obtained. The difference between $Y_i(1)$ and $Y_i(2)$ is calculated and defined as impact value I_i, as depicted in Eq. (7)-(9).

$$Y_i(1) = \begin{bmatrix} y_{11}(1) & y_{12}(1) & \ldots & y_{1m}(1) \\ \vdots & \vdots & & \vdots \\ y_{k1}(1) & y_{k2}(1) & \ldots & y_{km}(1) \\ \vdots & \vdots & \ddots & \vdots \\ y_{l1}(1) & y_{l2}(1) & \cdots & y_{lm}(1) \end{bmatrix} \tag{7}$$

$$Y_i(2) = \begin{bmatrix} y_{11}(2) & y_{12}(2) & \ldots & y_{1m}(2) \\ \vdots & \vdots & & \vdots \\ y_{k1}(2) & y_{k2}(2) & \ldots & y_{km}(2) \\ \vdots & \vdots & \ddots & \vdots \\ y_{l1}(2) & y_{l2}(2) & \cdots & y_{lm}(2) \end{bmatrix} \tag{8}$$

$$I_i = Y_i(2) - \ Y_i(1) \tag{9}$$

,where, l is the number of the output variable.

(4) The MIV of ith input variable on the kth output variable could be calculated according to Eq. (10). The sequence of the input variables is sorted according to their absolute MIVs.

$$MIV_i(k) = \frac{1}{m}\sum_{j=1}^{m}(I_i)_{kj} \tag{10}$$

(5) The contribution rate to the kth output variable from the ith input variable can be further calculated as following[40]:

$$C_i(k) = \frac{|MIV_i(k)|}{\sum_{i=1}^{n}|MIV_i(k)|} * 100\% \tag{11}$$

4. Results and discussions

4.1 Analysis of the coating properties

As displayed in Tabel.2, the microhardness of coatings varies from 461±33 to 732±48 $HV_{0.3}$. The operating parameters of stand-off distance of 280 mm, O_2 flow rate of 200 slpm, and CH_4 flow rate of 160 slpm contributes to the highest microhardness of 732±48 $HV_{0.3}$. Higher values of microhardness mainly occur with relatively short stand-off distance (280 mm). For the distribution of the porosity of coatings, it mainly concentrates in the range of 0.67±0.12% to 1.78±0.31%. Most of the relatively higher values of the coatings porosities are related to shorter stand-off distance (280 mm), especially with lower O_2 flow rate of 200 slpm. For the wear rate of coatings during the abrasion test, it distributes randomly and mainly focuses on the range of $4.00\pm1.30\times10^5$ to $15.73\pm1.95\times10^5$ $mm^3/N/m$. A relatively low coating wear rate occurs when the stand-off distance is 280 mm and the O_2 flow rate of is 240 slpm.

The stand-off distance has a greater impact on the coating properties which has a relatively slighter fluctuation with the varied of the flow rate of O_2 and CH_4. However, there are no obviously relationships among the microhardness, the porosity and the wear rate of the coatings.

In addition, it is hard to build the relationship between the process parameters of HVOF spray and the coatings performances by curve fitting. Therefore, an ANN model is needed to further investigate and predict the performance of coatings.

4.2 Analysis of the training and validation process of ANN model

The ANN model was trained more than 100 times and the one generating the minimum error of the validation set was saved. An R-value of 0.99965 for the ANN model to predict the coating properties from the process parameters of the HVOF process was obtained. The R-value provides an understanding of how well the network was trained. The training result demonstrating the comparison between the targets (*T*, experimental values) and outputs (*y*, predicted values) of the ANN model was shown in Fig.2. The line y = T represents that the predicted outputs exactly match the targets. It is clear that all of the data standing for the microhardness, porosity and wear rate of coatings are dispersed around the line y = T, which indicates that the trained result rightly fit with the targets. This can be further verified by the relatively small absolute errors (maximum error of 2.675%) from the error histogram, as displayed in Fig.3.

The predicted outputs of the ANN model were inverse normalized after training to compare with the experimental values. As displayed in Fig.4, the comparison between the experimental values and the predicted values of the training and validation set of the ANN model was given, where the red and blue symbols stand for the experimental and predicted values, respectively. In the first approximation, results are in good agreement. The relative errors between the experimental values and the predicted values were calculated with respect to the experimental values and shown in Fig.5. As shown in Fig.5(a), the relative error between the experimental and predicted values of the microhardness of coatings varies from -0.703% to 1.538% with an average of 0.156% and a standard deviation of 0.477%. It distributes smaller and more concentrated than the porosity of coatings varying from -0.535% to 2.062% with an average of 0.239% and a standard deviation of 0.605% (shown in Fig.5(b)). The wear rate of coatings shows

the widest and the most discrete distribution with a range from -4.361% to 4.407%, an average of 0.004% and standard deviation of 1.922%, as displayed in Fig.5(c)). It indicates that the ANN model is more accurate in predicting the microhardness of coatings, which is mainly attributed to the more regular tendency of the distribution of coatings microhardness.

4.3 Testing of ANN model

The test set of ANN model (No. 3, 4 and 19), randomly allocated from the data set in Table.III, is independent from the training and optimization process of the ANN model. Its predicted and experimental values was inverse normalized and shown in Fig.6, where the black and red columns stand for the predicted and experimental values, respectively. As shown in Fig.6, the maximum of the relative errors for the microhardness, porosity and wear rate of coatings are 1.513%, 0.715% and 1.552%, corresponding to a difference of 9.17 $HV_{0.3}$, 0.01 %area, and 0.11×10^{-5} $mm^3/N/m$. The minimums of the relative errors are 0.157%, 0.039% and 0.085%%, respectively. It can be seen that the predicted values are consistent with the experimental values and the range of the relative errors in test set is smaller than that of training and validation set. Analysis suggests that the ANN model is properly trained to predict the microhardness, porosity and wear rate of coatings from the HVOF sprayed process parameters. Though the relationships between the HVOF sprayed process parameters and the properties of coating are complex, it is possible to directly predict the coating properties by employing the ANN model.

4.4 MIV based analysis for the ANN model

The MIV based analysis method has been widely accepted as one of the best indicators for evaluating the value of a given coefficient for an ANN model [37,41,42]. The MIV value and contribution rate for each input variable on each output variable were calculated and shown in Table.V and Table.Ⅵ. Results show that the important sequence of the factors for the

microhardness and porosity is: spray distance > O_2 flow rate > CH_4 flow rate; for the wear rate: O_2 flow rate > spray distance > CH_4 flow rate. Spray distance is the most important factor to influence the microhardness and porosity, which occupies 50% and 57% contribution rate, respectively. This result keeps consistency with the analysis of the coating properties in Section 4.1. However, the importance of O_2 flow rate is much more than spray distance for the wear rate, possessing 57% contribution rate. CH_4 flow rate always has the slightest impact on all output variables, contributing 17%, 18% and 20% for microhardness, porosity and wear rate of coating, respectively.

Though the fuel in the HVOF spray is different from this study, previous works have also concluded that the spray distance performs greater influence on the microhardness and porosity of coatings than the oxygen flow rate for different kinds of feedstock [14,43,44]. Another study has also been carried out to emphasize the great influence of spray distance on coatings microhardness from the perspective of airborne acoustic emission during the HVOF spray[45]. Research [46] also suggested that the oxygen flow rate has complex impact on the coatings wear performance. On the one hand, the increase of the oxygen flow rate would increase the velocity of particle in-flight and enhance the cooling effect for the particle in-flight, resulting in the decrease of the temperature of particle in-flight, which would decrease the coatings wear resistance. On the other hand, increasing the oxygen flow rate would contribute to increasing the temperature of particle in-flight due to increasing the reaction rate of the gases. Unfortunately, there are limited researches to directly compare the importance of the process parameters. In this work, The MIV based analysis makes up the study of the importance of the process parameters, especially for ANN model.

5. Conclusions

In this work, an ANN model has been configured, trained and optimized to predict the coating properties (i.e. microhardness, porosity and wear rate of coating) from the operating

parameters of HVOF spray(i.e. stand-off distance, flow rate of CH_4 and O_2). HVOF spray experiments and related tests were conducted to set up the data set for the training, validation and test of the ANN model. The ANN model has been trained and optimized. An R-value of 0.99965 with a maximum error of 2.675% is achieved to verify the prediction performance of the ANN model. The reliability and accuracy of the ANN model have been further verified by the test sets, where the relative errors are smaller than the maximum errors of the training and validation set (1.538%, 2.062% and 9.407% for microhardness, porosity and wear rate of coating, respectively). Therefore, the developed ANN model can be used for spray behavior prediction and further parameter control or optimization in coating operating practice. Additionally, the MIV based analysis has been carried out for evaluating the factors importance. Results show that the important sequence of the factors for the microhardness and porosity is: spray distance > O_2 flow rate > CH_4 flow rate; for the wear rate: O_2 flow rate > spray distance > CH_4 flow rate.

Acknowledgments

The authors gratefully appreciate the support from the China Scholarship Council (Grant No. 201604490072, No. 201504490038, and No. 201701810152).

References

[1] F.J. Hermanek, Thermal spray terminology and company origins, ASM international, 2001.

[2] A. Dolatabadi, V. Pershin, J. Mostaghimi, New attachment for controlling gas flow in the HVOF process, Journal of Thermal Spray Technology. 14 (2005) 91–99.

[3] L. Pawlowski, The Science and Engineering of Thermal Spray Coatings, John Wiley & Sons, 2008.

[4] M.L. Thorpe, H.J. Richter, A pragmatic analysis and comparison of HVOF processes, Journal of Thermal Spray Technology. 1 (1992) 161–170.

[5] J. Vicenzi, C.M. Marques, C.P. Bergmann, Hot and cold erosive wear of thermal sprayed NiCr-based coatings: Influence of porosity and oxidation, Surf. Coat. Technol. 202 (2008) 3688–3697. doi:10.1016/j.surfcoat.2008.01.010.

[6] D. Poirier, J.-G. Legoux, R.S. Lima, Engineering HVOF-Sprayed Cr3C2-NiCr Coatings: The Effect of Particle Morphology and Spraying Parameters on the Microstructure, Properties, and High Temperature Wear Performance, J Therm Spray Tech. 22 (2013) 280–289. doi:10.1007/s11666-012-9833-3.

[7] V. Matikainen, G. Bolelli, H. Koivuluoto, M. Honkanen, M. Vippola, L. Lusvarghi, P. Vuoristo, A Study of Cr3C2-Based HVOF-and HVAF-Sprayed Coatings: Microstructure and Carbide Retention, Journal of Thermal Spray Technology. 26 (2017) 1239–1256.

[8] A.S. Kang, J.S. Grewal, G.S. Cheema, Effect of thermal spray coatings on wear behavior of high tensile steel applicable for tiller blades, Materials Today: Proceedings. 4 (2017) 95–103.

[9] N. Vashishtha, R.K. Khatirkar, S.G. Sapate, Tribological behaviour of HVOF sprayed WC-12Co, WC-10Co-4Cr and Cr3C2– 25NiCr coatings, Tribology International. 105 (2017) 55–68.

[10] J. Saaedi, T.W. Coyle, H. Arabi, S. Mirdamadi, J. Mostaghimi, Effects of HVOF process parameters on the properties of Ni-Cr coatings, Journal of Thermal Spray Technology. 19 (2010) 521–530.

[11] V. Matikainen, H. Koivuluoto, P. Vuoristo, J. Schubert, Š. Houdková, Effect of Nozzle Geometry on the Microstructure and Properties of HVAF-Sprayed WC-10Co4Cr and Cr 3 C 2-25NiCr Coatings, Journal of Thermal Spray Technology. 27 (2018) 680–694.

[12] I. López Báez, C.A. Poblano Salas, J. Muñoz Saldaña, L.G. Trápaga Martínez, Effects of the Modification of Processing Parameters on Mechanical Properties of HVOF Cr2C3-25NiCr Coatings, J Therm Spray Tech. 24 (2015) 938–946. doi:10.1007/s11666-015-0255-x.

[13] X. Guo, M.-P. Planche, J. Chen, H. Liao, Relationships between in-flight particle characteristics and properties of HVOF sprayed WC-CoCr coatings, Journal of Materials Processing Technology. 214 (2014) 456–461.

[14] A.S. Praveen, J. Sarangan, S. Suresh, B.H. Channabasappa, Optimization and erosion wear response of NiCrSiB/WC–Co HVOF coating using Taguchi method, Ceramics International. 42 (2016) 1094–1104.

[15] L. Qiao, Y. Wu, S. Hong, J. Zhang, W. Shi, Y. Zheng, Relationships between spray parameters, microstructures and ultrasonic cavitation erosion behavior of HVOF sprayed Fe-based amorphous/nanocrystalline coatings, Ultrasonics Sonochemistry. 39 (2017) 39–46.

[16] J. Singh, S. Kumar, G. Singh, Taguchi's Approach For Optimization Of Tribo-Resistance Parameters Forss304, Materials Today: Proceedings. 5 (2018) 5031–5038.

[17] M. Li, P.D. Christofides, Modeling and Control of High-Velocity Oxygen-Fuel (HVOF) Thermal Spray: A Tutorial Review, J Therm Spray Tech. 18 (2009) 753. doi:10.1007/s11666-009-9309-2.

[18] E. Dongmo, M. Wenzelburger, R. Gadow, Analysis and optimization of the HVOF process by combined experimental and numerical approaches, Surface and Coatings Technology. 202 (2008) 4470–4478. doi:10.1016/j.surfcoat.2008.04.029.
[19] H. Tabbara, S. Gu, D.G. McCartney, Computational modelling of titanium particles in warm spray, Computers & Fluids. 44 (2011) 358–368. doi:10.1016/j.compfluid.2011.01.034.
[20] A.J. Maren, C.T. Harston, R.M. Pap, Handbook of Neural Computing Applications, Academic Press, 2014.
[21] W.S. McCulloch, W. Pitts, A logical calculus of the ideas immanent in nervous activity, The Bulletin of Mathematical Biophysics. 5 (1943) 115–133.
[22] S. Agatonovic-Kustrin, R. Beresford, Basic concepts of artificial neural network (ANN) modeling and its application in pharmaceutical research, Journal of Pharmaceutical and Biomedical Analysis. 22 (2000) 717–727. doi:10.1016/S0731-7085(99)00272-1.
[23] H. Taghavifar, S. Khalilarya, S. Jafarmadar, Diesel engine spray characteristics prediction with hybridized artificial neural network optimized by genetic algorithm, Energy. 71 (2014) 656–664.
[24] S. Guessasma, Z. Salhi, G. Montavon, P. Gougeon, C. Coddet, Artificial intelligence implementation in the APS process diagnostic, Materials Science and Engineering: B. 110 (2004) 285–295.
[25] S. Guessasma, G. Montavon, C. Coddet, Neural computation to predict in-flight particle characteristic dependences from processing parameters in the APS process, J Therm Spray Tech. 13 (2004) 570–585. doi:10.1361/10599630419391.
[26] S. Guessasma, F.-I. Trifa, G. Montavon, C. Coddet, Al2O3–13% weight TiO2 deposit profiles as a function of the atmospheric plasma spraying processing parameters, Materials & Design. 25 (2004) 307–315. doi:10.1016/j.matdes.2003.10.019.
[27] A.-F. Kanta, G. Montavon, C.C. Berndt, M.-P. Planche, C. Coddet, Intelligent system for prediction and control: Application in plasma spray process, Expert Systems with Applications. 38 (2011) 260–271.
[28] T. Liu, M.P. Planche, A.F. Kanta, S. Deng, G. Montavon, K. Deng, Z.M. Ren, Plasma Spray Process Operating Parameters Optimization Based on Artificial Intelligence, Plasma Chemistry and Plasma Processing. 33 (2013) 1025–1041.
[29] H. Çetinel, H. Öztürk, E. Çelik, B. Karlık, Artificial neural network-based prediction technique for wear loss quantities in Mo coatings, Wear. 261 (2006) 1064–1068. doi:10.1016/j.wear.2006.01.040.
[30] M.A.R. Mojena, A.S. Roca, R.S. Zamora, M.S. Orozco, H.C. Fals, C.R.C. Lima, Neural network analysis for erosive wear of hard coatings deposited by thermal spray: Influence of microstructure and mechanical properties, Wear. 376 (2017) 557–565.
[31] G. Zhang, A.-F. Kanta, W.-Y. Li, H. Liao, C. Coddet, Characterizations of AMT-200 HVOF NiCrAlY coatings, Materials & Design. 30 (2009) 622–627.
[32] D. Zissis, E.K. Xidias, D. Lekkas, A cloud based architecture capable of perceiving and predicting multiple vessel behaviour, Applied Soft Computing. 35 (2015) 652–661.
[33] T.A. Choudhury, N. Hosseinzadeh, C.C. Berndt, Artificial Neural Network application for predicting in-flight particle characteristics of an atmospheric plasma spray process, Surface and Coatings Technology. 205 (2011) 4886–4895. doi:10.1016/j.surfcoat.2011.04.099.
[34] M.A. Nielsen, Neural networks and deep learning, Determination press USA, 2015.
[35] M.H. Beale, M.T. Hagan, H.B. Demuth, Neural Network Toolbox™ User's Guide, The Mathworks Inc. (1992).
[36] G.W. Dombi, P. Nandi, J.M. Saxe, A.M. Ledgerwood, C.E. Lucas, Prediction of rib fracture injury outcome by an artificial neural network, Journal of Trauma and Acute Care Surgery. 39 (1995) 915–921.

[37] J.-L. Jiang, X. Su, H. Zhang, X.-H. Zhang, Y.-J. Yuan, A novel approach to active compounds identification based on support vector regression model and mean impact value, Chemical Biology & Drug Design. 81 (2013) 650–657.
[38] J.-L. Jiang, Z.-D. Li, H. Zhang, Y. Li, X.-H. Zhang, Y. Yuan, Y. Yuan, Feature Selection for the Identification of Antitumor Compounds in the Alcohol Total Extracts of Curcuma longa, Planta Med. 80 (2014) 1036–1044. doi:10.1055/s-0034-1382951.
[39] X. Jiang, J. Hu, M. Jia, Y. Zheng, Parameter matching and instantaneous power allocation for the hybrid energy storage system of pure electric vehicles, Energies. 11 (2018) 1933.
[40] G. Xu, P. Schwarz, H. Yang, Determining China's CO2 emissions peak with a dynamic nonlinear artificial neural network approach and scenario analysis, Energy Policy. 128 (2019) 752–762.
[41] Y.-R. Zeng, Y. Zeng, B. Choi, L. Wang, Multifactor-influenced energy consumption forecasting using enhanced back-propagation neural network, Energy. 127 (2017) 381–396.
[42] M. Qi, Z. Fu, F. Chen, Research on a feature selection method based on median impact value for modeling in thermal power plants, Appl. Therm. Eng. 94 (2016) 472–477. doi:10.1016/j.applthermaleng.2015.10.104.
[43] Q. Wang, Z. Chen, L. Li, G. Yang, The parameters optimization and abrasion wear mechanism of liquid fuel HVOF sprayed bimodal WC–12Co coating, Surface and Coatings Technology. 206 (2012) 2233–2241.
[44] W. Tillmann, E. Vogli, I. Baumann, G. Kopp, C. Weihs, Desirability-based multi-criteria optimization of HVOF spray experiments to manufacture fine structured wear-resistant 75Cr 3 C 2-25 (NiCr20) coatings, Journal of Thermal Spray Technology. 19 (2010) 392–408.
[45] S. Kamnis, K. Malamousi, A. Marrs, B. Allcock, K. Delibasis, Aeroacoustics and Artificial Neural Network Modeling of Airborne Acoustic Emissions During High Kinetic Energy Thermal Spraying, J Therm Spray Tech. 28 (2019) 946–962. doi:10.1007/s11666-019-00874-0.
[46] C.-J. Li, G.-C. Ji, Y.-Y. Wang, K. Sonoya, Dominant effect of carbide rebounding on the carbon loss during high velocity oxy-fuel spraying of Cr3C2–NiCr, Thin Solid Films. 419 (2002) 137–143. doi:10.1016/S0040-6090(02)00708-3.

Table.I Examples of ANN models used in thermal spray

Spray technique	Spray material	Inputs	Outputs	Reference
Atmospheric plasma spray (APS)	Al_2O_3–13% Weight TiO_2	Arc current intensity; injector stand-off distance; injector diameter; carried gas flow rate; H_2 flow rate; Ar flow rate	Particle temperature, particle velocity, particle diameter	(Ref 24,25)
APS	Al_2O_3–13% Weight TiO_2	Arc current intensity; total gas(H_2 + Ar); H_2 content(H_2/Ar); carried gas flow rate; injector diameter	Height and the flattening of the coating profile	[26]
APS	Al_2O_3–13% Weight TiO_2	Arc current intensity; total gas(H_2 + Ar); H_2 content(H_2/Ar); carried gas flow rate	Particle temperature, particle velocity	[27]
APS	Al_2O_3–13% Weight TiO_2	Particle temperature; particle velocity	Coating porosity	[28]
APS	Mo (Metco) powders	Wear environment (dry and acidic); normal load; wear time	Microhardness and the amount of wear loss	[29]
HVOF and flame spray	WC-CoCr, Cr3C2-NiCr,	Deposition method; impact angle and speed of abrasive particles; fracture toughness; microhardness; porosity; roughness; coating density	Erosion rate	[30]
HVOF spray	NiCrAlY	O_2 flow rate; spraying distance	Coating porosity and hardness	[31]

Table.II HVOF spray process parameters

Parameters	Values
O_2 flow rate (slpm)	200, 240
CH_4 flow rate (slpm)	120, 140, 160, 180, 200
Air flow rate (slpm)	300
Carrier gas flow rate (slpm)	40
Stand-off distance (mm)	280, 320
Gun traverse speed (mm/s)	200
Powder feed rate (g/min)	30

Table.III Database for the training, validation and test of the ANN model

No.	HVOF process parameters			Coating porosities		
	Dis [mm]	$Q(O_2)$ [slpm]	$Q(CH_4)$ [slpm]	Microhardness [$HV_{0.3}$]	Porosity [%area]	Wear rate$\times10^{-5}$ [mm³/N/m]
1	280	200	120	558±39	1.47±0.23	15.59±1.56
2	280	200	140	531±20	1.37±0.28	7.12±1.73
3	280	200	160	732±48	1.78±0.31	6.12±1.46
4	280	200	180	606±50	1.70±0.16	10.17±1.54
5	280	200	200	575±56	1.23±0.19	11.74±2.26
6	280	240	120	532±51	1.56±0.24	10.25±1.20
7	280	240	140	561±36	0.87±0.20	4.20±2.16
8	280	240	160	691±42	1.00±0.17	4.47±1.14
9	280	230	180	632±58	1.03±0.23	5.00±0.86
10	280	225	200	656±35	0.83±0.33	4.00±1.30
11	320	200	120	461±33	1.11±0.21	4.95±0.91
12	320	200	140	474±36	0.92±0.18	9.15±2.81
13	320	200	160	531±45	0.67±0.12	9.70±1.61
14	320	200	180	547±31	0.86±0.12	7.69±0.93
15	320	200	200	565±18	0.98±0.31	8.92±3.06
16	320	240	120	509±33	0.88±0.14	15.73±3.95
17	320	240	140	596±43	0.72±0.20	9.93±3.04
18	320	240	160	557±34	0.80±0.09	5.54±1.57
19	320	233	180	606±41	0.99±0.08	6.94±1.65
20	320	230	200	583±39	0.87±0.17	6.88±1.66

Table.IV Training functions of the ANN model

functions	**Values**
Pre-processing and post-processing function	mapminmax removeconstantrows
data division function	dividerand
Transfer function for hidden layers	logsig
Transfer function for the output layer	purelin
Training function	trainlm

Table.V The MIV values for input variables

Input variables	**Output variables**		
	Microhardness	porosity	Wear rate
Distance	-0.128	-0.273	-0.076
$Q(O_2)$	0.085	-0.118	-0.189
$Q(CH_4)$	0.045	-0.086	-0.068

Table.Ⅵ The contribution rate for input variables

Input variables	**Output variables**		
	Microhardness	porosity	Wear rate
Distance	50%	57%	23%
$Q(O_2)$	33%	25%	57%
$Q(CH_4)$	17%	18%	20%

Figure captions

Fig.1 The architecture of the ANN model

Fig.2 The comparison between the output and the target

Fig.3 The error histogram of the training results

Fig.4 The comparison of the predicted and experimental result of microhardness (a), porosity (b), and wear rate (c) of coatings in training and validation set

Fig.5 The distribution of relative errors of microhardness (a), porosity (b), and wear rate (c) of coatings in training and validation set

Fig.6 The comparison of the predicted and experimental result of microhardness (a), porosity (b), and wear rate (c) of coatings in test set

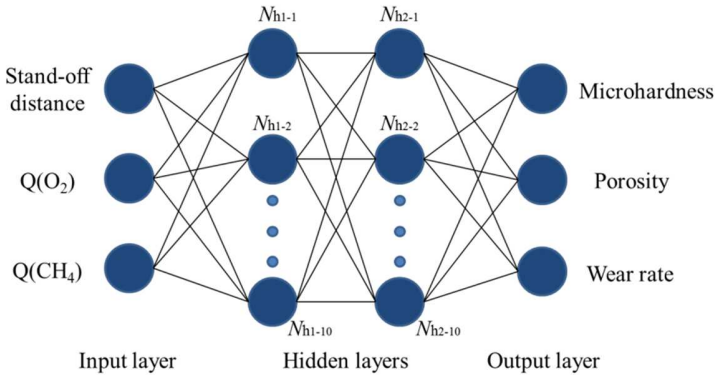
N_{h1-1}
N_{h2-1}
Stand-off distance
N_{h1-2}
N_{h2-2}
Microhardness
$Q(O_2)$
Porosity
$Q(CH_4)$
Wear rate
N_{h1-10}
N_{h2-10}
Input layer
Hidden layers
Output layer

Fig.1

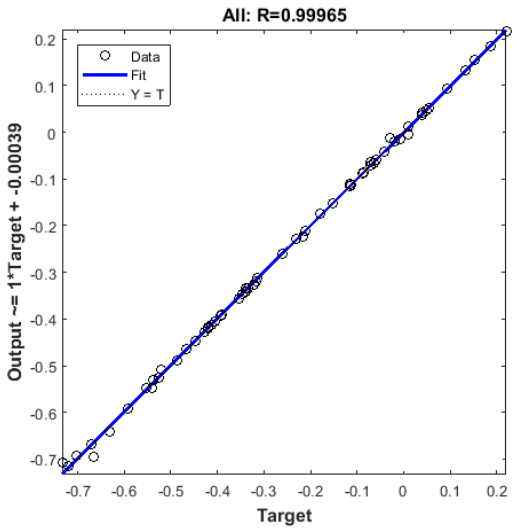
All: R=0.99965
Data
Fit
Y = T
Output ~= 1*Target + -0.00039
Target
0.2
0.1
0
-0.1
-0.2
-0.3
-0.4
-0.5
-0.6
-0.7
-0.7
-0.6
-0.5
-0.4
-0.3
-0.2
-0.1
0
0.1
0.2

Fig.2

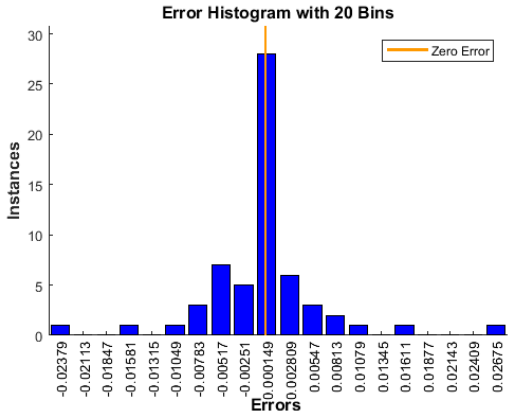
Error Histogram with 20 Bins
Zero Error
Instances
Errors
30
25
20
15
10
5
0
-0.02379
-0.02113
-0.01847
-0.01581
-0.01315
-0.01049
-0.00783
-0.00517
-0.00251
0.000149
0.002809
0.00547
0.00813
0.01079
0.01345
0.01611
0.01877
0.02143
0.02409
0.02675

Fig.3

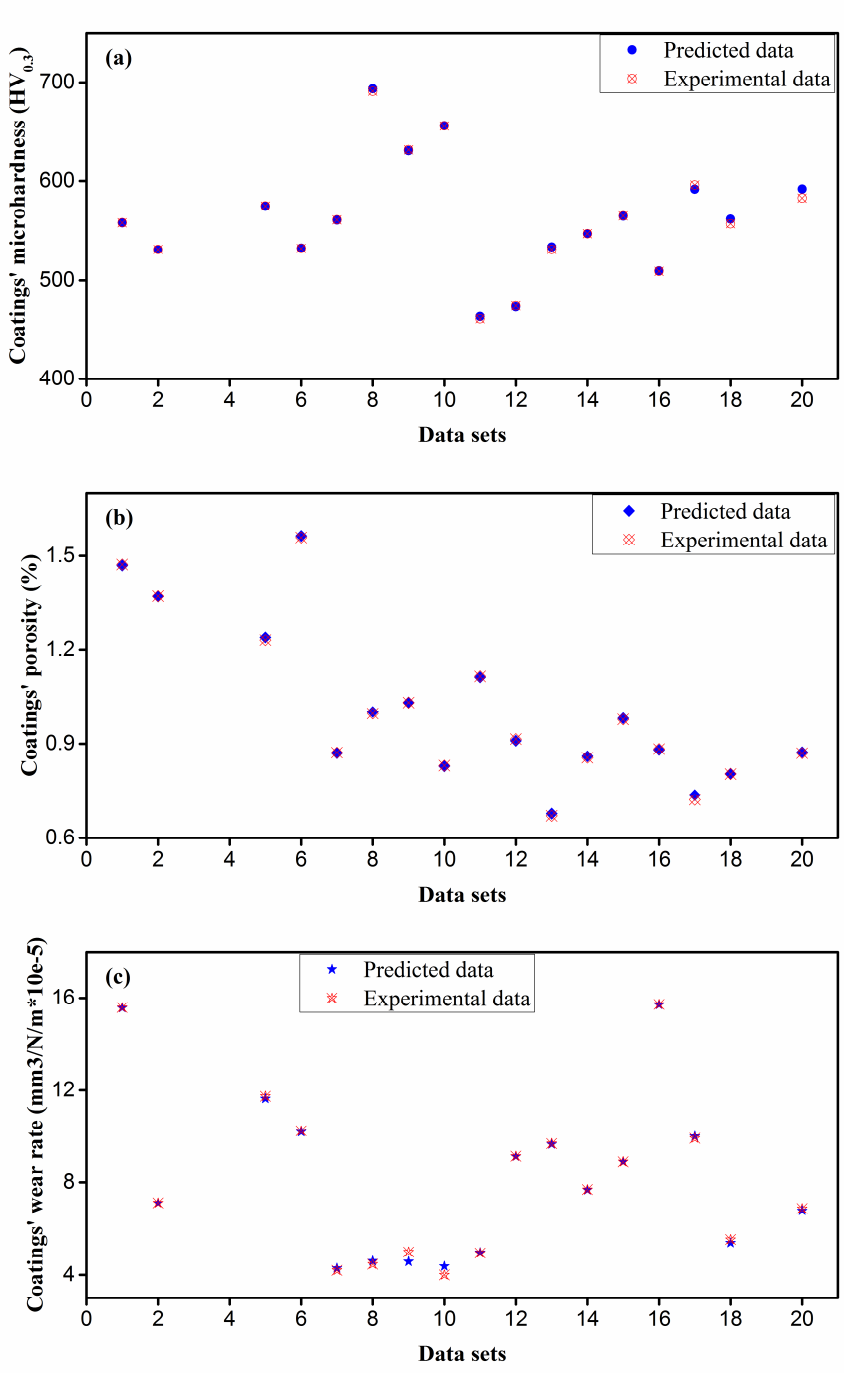
(a)
Predicted data
Experimental data
Coatings' microhardness (HV0.3)
Data sets
(b)
Predicted data
Experimental data
Coatings' porosity (%)
Data sets
(c)
Predicted data
Experimental data
Coatings' wear rate (mm3/N/m*10e-5)
Data sets

Fig.4

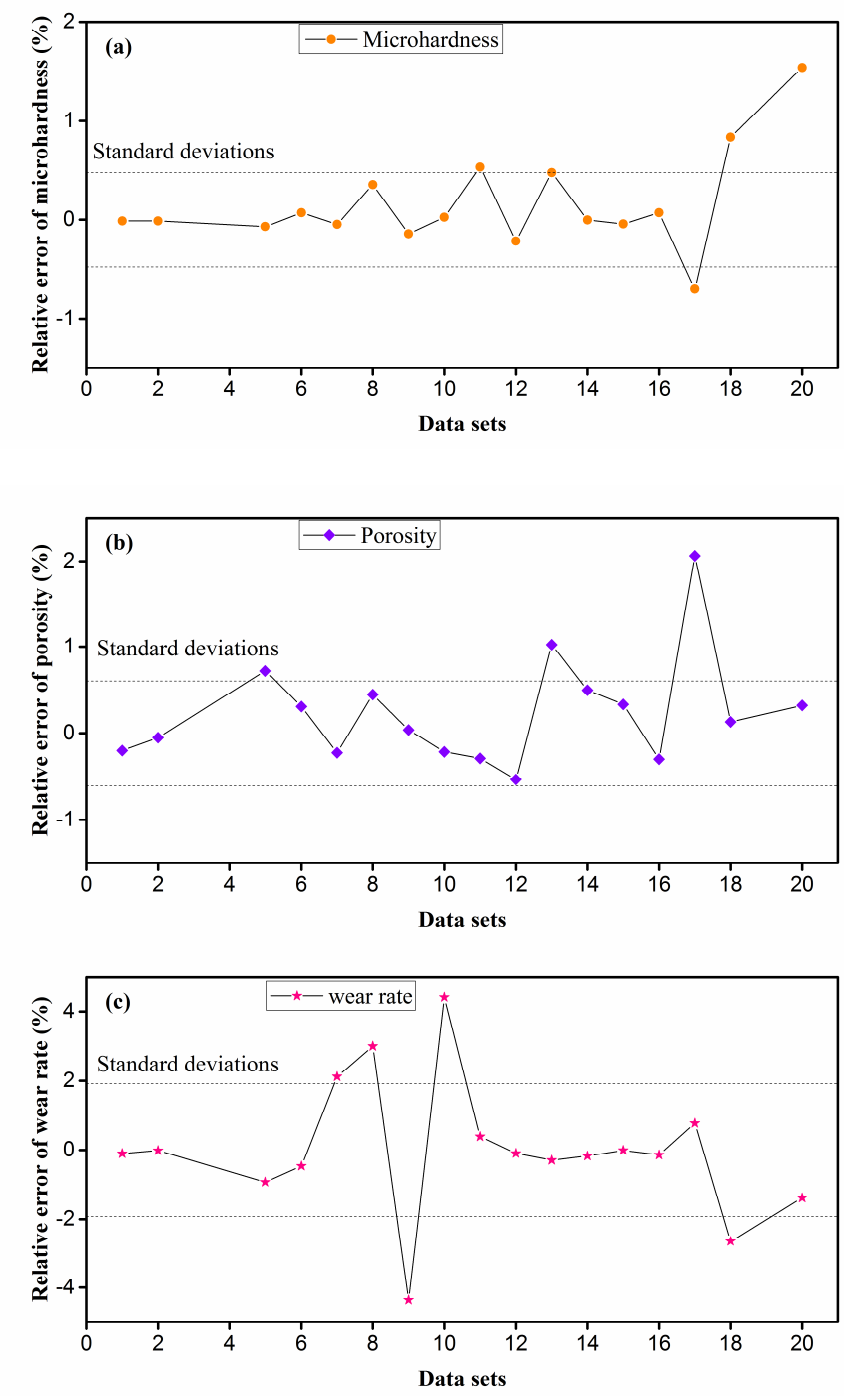
(a)
Microhardness
Standard deviations
Relative error of microhardness (%)
Data sets
(b)
Porosity
Standard deviations
Relative error of porosity (%)
Data sets
(c)
wear rate
Standard deviations
Relative error of wear rate (%)
Data sets

Fig.5

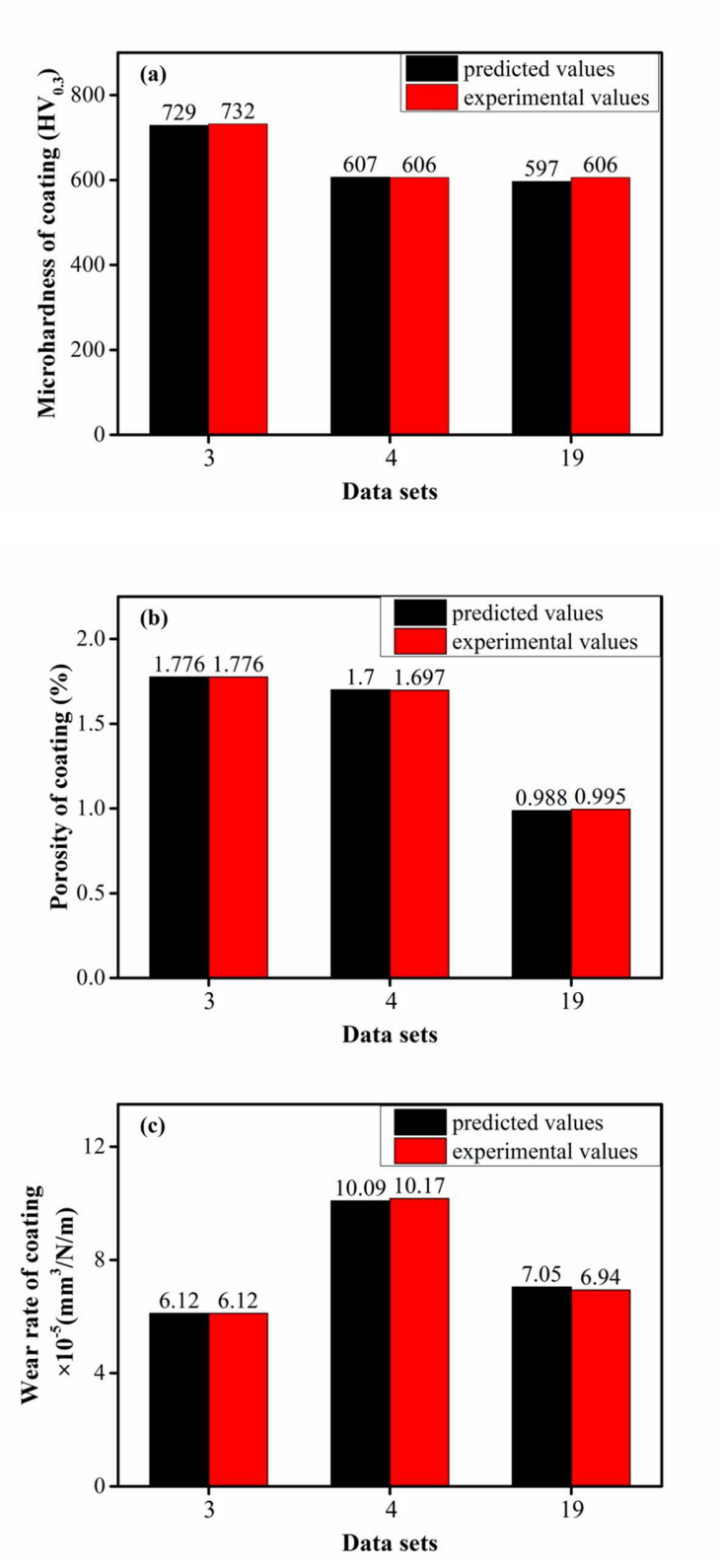
(a)
predicted values
experimental values
Microhardness of coating ($HV_{0.3}$)
729 732
607 606
597 606
0 200 400 600 800
3 4 19
Data sets
(b)
predicted values
experimental values
Porosity of coating (%)
1.776 1.776
1.7 1.697
0.988 0.995
0.0 0.5 1.0 1.5 2.0
3 4 19
Data sets
(c)
predicted values
experimental values
Wear rate of coating ×10^{-5}(mm^3/N/m)
6.12 6.12
10.09 10.17
7.05 6.94
0 4 8 12
3 4 19
Data sets

Fig.6